Phase-matched high-order harmonic generation and parametric amplification

S. Meyer, B. N. Chichkov,* and B. Wellegehausen
Institut für Quantenoptik, Universität Hannover Welfengarten 1, D-30167 Hannover, Germany

A. Sanpera
Institut für Theoretische Physik, Universität Hannover Appelstraße 2, D-30167 Hannover, Germany

(Received 4 October 1999; published 16 May 2000)

Investigations of high-order harmonic generation and frequency mixing in absorbing and dispersive media are reported. Detailed analysis of propagation effects and factors limiting the frequency conversion efficiency is given. Experimental results obtained by us and other groups are discussed and compared with calculations. The development of high-order parametric amplifiers as a new possibility to solve the frequency conversion problem is analyzed.

PACS number(s): 42.65.Ky, 32.80.Wr, 42.65.Re

I. INTRODUCTION

For the efficient generation of high-order harmonics with ultrashort laser pulses, it is of principle importance to have a perfect phase matching between the driving laser pulse and the generated harmonic signal. This topic has attracted considerable attention during the last years [1–13]. In [4], it has been demonstrated that high-order difference-frequency mixing can be phase matched in weakly ionized plasmas. Later, phase matching has been observed in gas-filled hollow-core fibers [8,13], gas jets [9], and self-guided laser beams [10]. But even in case of perfect phase matching the harmonic output is limited. Therefore, the improvement of the high-order harmonic generation efficiency (well above 10^{-5}) remains a challenging problem.

In this paper, all factors limiting the high-order harmonic generation efficiency are discussed. Taking them into account a very good agreement between calculations and experimental results is obtained. In Sec. II, which has an introduction, a ''practical'' phase-matching condition and expressions for maximum high-order harmonic intensities and conversion efficiencies are derived. In Sec. III, evolution of the nonlinear refractive index during the laser pulse is analyzed. In this section we also define optimum laser intensities required for an efficient generation of a certain harmonic and show that the pulse duration of this harmonic can be in the attosecond range. In Sec. IV and Sec. V, effects of geometrical (or fiber) phase mismatch and of attenuation of the pump wave are discussed. A review of some recent experiments together with our calculations is given in Sec. VI. The experimental setup and results obtained by our group are presented in Sec. VII. In Sec. VIII, prospects for the development of high-order parametric generators and amplifiers operating in the extreme ultraviolet (XUV) spectral range are analyzed.

II. HARMONICS IN DISPERSIVE AND ABSORBING MEDIA

Throughout this paper we use the slowly varying envelope approximation for the pump laser field $E_1(z,t)$ and for the generated field $E(z,t)$

$$E_1(z,t)=\frac{1}{2}A_1(z,t)\exp[i(k_1z-\omega_1t)]+\text{c.c.},$$
$$E(z,t)=\frac{1}{2}\sum_q A_q(z,t)\exp[i(k_qz-\omega_qt)]+\text{c.c.}, \tag{1}$$

where k_1, k_q are the wave vectors and ω_1, ω_q are the frequencies of the pump wave and of the q-order harmonic, respectively. In this approximation the generation of the q-order harmonic can be described by

$$\frac{dA_q}{dz}+\frac{\alpha_q}{2}A_q=i\gamma_q\exp[-i\Delta k_qz], \tag{2}$$

where α_q is the absorption coefficient, $\Delta k_q=k_q-qk_1$ is the wave-vector mismatch, and γ_q is the nonlinear driving term

$$\gamma_q=\frac{2\pi\omega_q}{cn_q}Nd_q^{NL}, \tag{3}$$

which is determined by the medium response to the applied laser field. Here d_q^{NL} is the amlitude of the nonlinear atomic dipole moment defined by $d_q(z,t)=(d_q^{NL}/2)\exp[iq(k_1-\omega_1t)]+\text{c.c.}$, N is the particle density, and n_q is the refractive index for the generated harmonic. In perturbation theory

$$Nd_q^{NL}=\frac{\chi^{(q)}}{2^{(q-1)}}A_1^q, \tag{4}$$

where $\chi^{(q)}$ is the susceptibility for the $\omega_q=q\omega_1$ process.

Solving Eq. (2) by integrating over the medium length L, we get for the intensity of the q-order harmonic $I_q=n_qc|A_q|^2/8\pi$

*Permanent address: P.N. Lebedev Physics Institute, Leninsky Prospect 53, Moscow, Russia.

$$I_q = \frac{\pi\omega_q^2}{2cn_q}|d_q^{NL}|^2 N^2 L^2 \exp(-\alpha_q L/2) \times \frac{\sin^2(\Delta k_q L/2)+\sinh^2(\alpha_q L/4)}{(\Delta k_q L/2)^2+(\alpha_q L/4)^2} = \frac{2\pi\omega_q^2}{cn_q}\frac{|d_q^{NL}|^2}{\sigma_q^2}F, \quad (5)$$

where $\sigma_q=\alpha_q/N$ is the absorption cross section and

$$F=\frac{4}{1+\delta^2}\exp(-\tau_q/2)[\sin^2(\delta\tau_q/4)+\sinh^2(\tau_q/4)] = \frac{1}{1+\delta^2}[1+\exp(-\tau_q)-2\cos(\delta\tau_q/2)\exp(-\tau_q/2)] \leqslant 1. \quad (6)$$

These expressions are analogous to that used in [9,13]. Here $\tau_q=\alpha_q L$ is the optical thickness for the q-order harmonic and $\delta=2\Delta k_q/\alpha_q$. The factor F determines the strength (intensity) of the harmonic signal. This factor is independent of the sign of the wave-vector mismatch Δk_q, which can be positive or negative depending on the medium dispersion. For large optical thicknesses $\tau_q \gg 1$, $F \simeq 1/(1+\delta^2)$.

The general dependence of the F factor on the parameters δ and τ_q is illustrated in Fig. 1(a). As can be seen, the maximum value $F=1$ can only be achieved for $\delta=0$. This corresponds to a perfect phase matching $\Delta k_q=0$ or to a strong absorption $\alpha_q \gg 2\Delta k_q$. For $\delta \neq 0$ the location of the maximum of the F function $\tau_q^{max}=(NL)^{max}\sigma_q$ and the maximum value $F(\tau_q^{max})$ are shown in Fig. 1(b). For practical purposes it is sufficient to have $F \geqslant 1/2$, which is fulfilled for $|\delta| \leqslant 1$ and $\tau_q \geqslant 3$, as can be seen in Fig. 1. Therefore, we can formulate a ''practical'' phase-matching condition as

$$|\Delta k_q|/N \leqslant \sigma_q/2 \quad \text{and} \quad N\sigma_q L \geqslant 3. \quad (7)$$

For sufficiently large absorption cross sections this ''practical'' condition can be easily realized. From this point the absorption is an ally because it simplifies the phase-matching requirements. On the other hand, for a process accompanied by a strong absorption it is impossible to obtain a high conversion efficiency, since the high-order harmonic intensity is inversly proportional to the square of the absorption cross section [see Eq. (5)].

The maximum high-order harmonic intensity (in the case of $F=1$) is determined by

$$I_q^{max}=\frac{8\pi^3 c}{n_q}\frac{|d_q^{NL}|^2}{\lambda_q^2\sigma_q^2}, \quad (8)$$

where $\lambda_q=\lambda_1/q$ is the wavelength of the q-order harmonic. Taking into account that the cross section of the pump laser beam is approximately q times larger than that of the q-order harmonic, we get for the maximum conversion efficiency $\eta^{max}=I_q^{max}/qI_1$, where I_1 is the pump laser intensity.

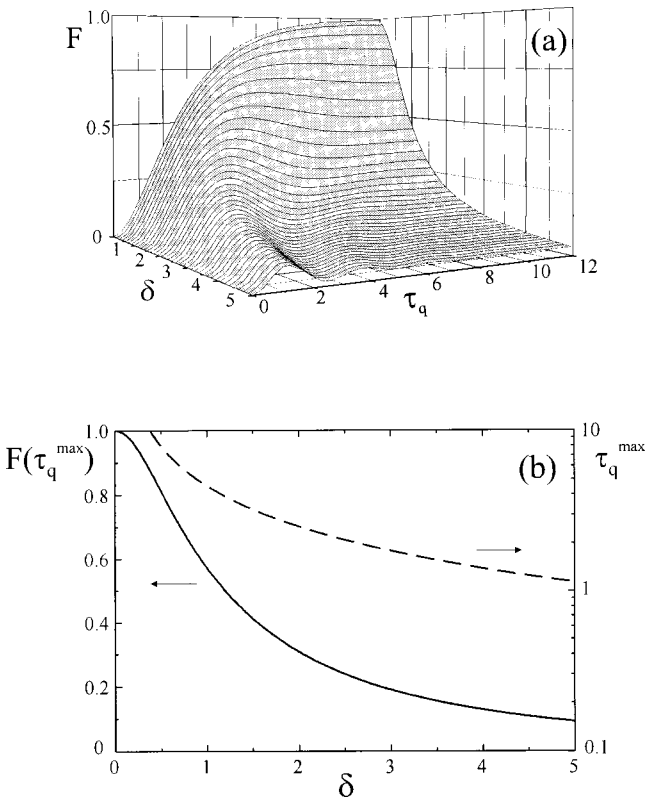

FIG. 1. (a) General dependence of the F factor (6) on the parameters $\delta=2\Delta k_q/\alpha_q$ and $\tau_q=\alpha_q L$. (b) Maximum value of this factor, $F(\tau_q^{max})$, and its location τ_q^{max}.

In Fig. 2 maximum conversion efficiencies that can be obtained in helium using as a pump 25 fs laser pulses at 400 nm are shown. In calculations the value of the nonlinear atomic dipole moment is found by solving numerically the time dependent Schrödinger equation in the single active electron approximation [14]. Photoabsorption cross sections are taken from Ref. [15].

III. NONLINEAR REFRACTIVE INDEX

In an intense laser field the refractive index $n(\lambda)$ becomes a function of time (or light intensity) due to the mutual action

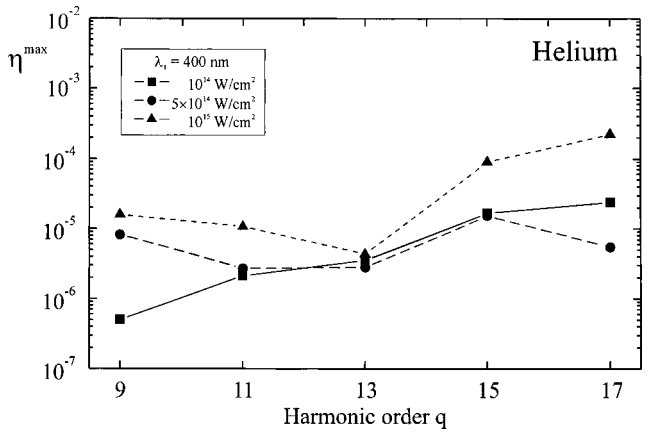

FIG. 2. Calculated maximum conversion efficiencies for harmonics generated by 25 fs, 400 nm laser pulses in helium.

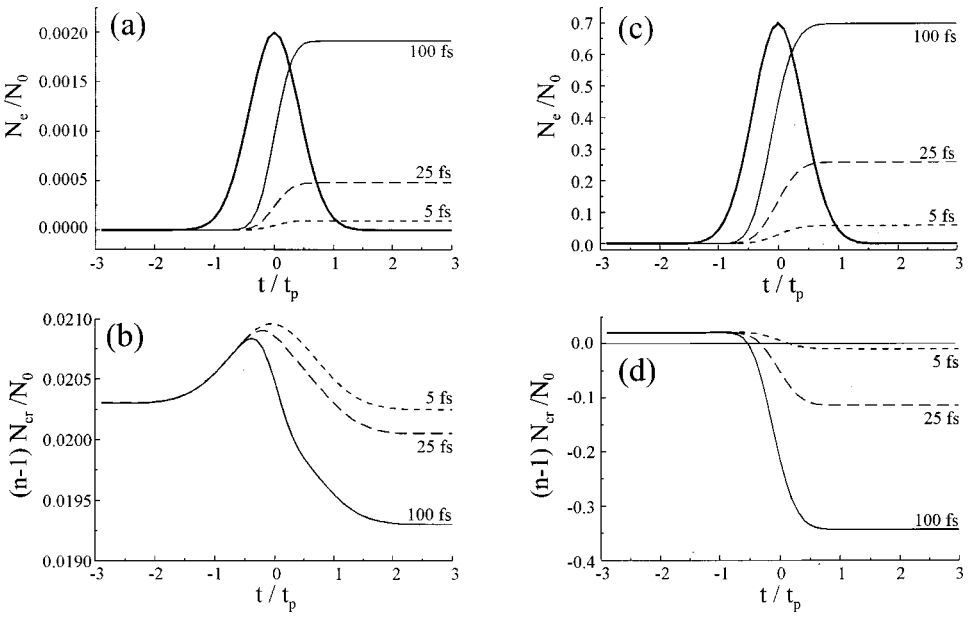

FIG. 3. Temporal evolution of the electron density N_e/N_0 and of the nonlinear refractive index $(n-1)N_{cr}/N_0$ during the laser pulse in argon. (a) and (c) Laser intensity profiles are shown by thick solid lines. Calculations are performed for two laser intensities (a) and (b) $I_1=8\times10^{13}$ W/cm^2 and (c) and (d) $I_1=2\times10^{14}$ W/cm^2 and different pulse durations (5 fs, 25 fs, and 100 fs).

of the Kerr effect and optical field ionization,

$$n(\lambda)-1=n_a(t)+n_i(t)+n_e(t), \tag{9}$$

where n_a, n_i, n_e are the atomic, ionic, and electronic contributions to the refrative index. These contributions are determined by

$$n_a(t)=\frac{\lambda^2}{2\pi}r_e N_a(t)\,\delta_a(\omega)+N_a(t)n_2^a(\lambda)I(t), \tag{10}$$

$$n_i(t)=\frac{\lambda^2}{2\pi}r_e N_i(t)\,\delta_i(\omega), \tag{11}$$

$$n_e(t)=-\frac{\lambda^2}{2\pi}r_e N_e(t), \tag{12}$$

where N_a, N_i, N_e are the corresponding particle densities, $r_e=e^2/mc^2=2.818\times10^{-13}$ cm is the classical electron radius, n_2^a is the single atom nonlinear refractive index coefficient, $n_2^a=n_2/2.4\times10^{19}$ (cm^5/W), and n_2 (in cm^2/W) is the Kerr coefficient at atmospheric pressure. $I(t)$ is the laser intensity, and

$$\delta_{(a,i)}(\omega)=\Re\left\{\sum_k^{(a,i)}\frac{\omega^2 f_{0k}}{\omega_{0k}^2-\omega^2+i\gamma_{0k}\omega}\right\} \tag{13}$$

describes dispersive characteristics of atoms or ions (the sum is performed over atomic or ionic transitions). The atomic contribution to the refractive index for the pump laser radiation is usually positive, whereas the free electron contribution is always negative. In our calculations below we neglect the ionic contribution completely, since usually the condition $\delta_i(\omega)\ll\delta_a(\omega)$ is fulfilled.

The temporal evolution of the particle densities during the laser pulse is described by optical field ionization

$$N_e(t)=N_0\left[1-\exp\left(-\int_{-\infty}^{t}W_{tun}(t')dt'\right)\right],$$
$$N_i(t)=N_e(t),\quad N_a(t)=N_0-N_e(t), \tag{14}$$

where N_0 is the initial atomic density, and W_{tun} is the probability of tunnel ionization in an intense laser field given by [16,17]

$$W_{tun}(t)=\omega_a\frac{(2l+1)}{8\pi}\frac{A(t)}{Z}P\left(\frac{4eZ^3}{n^{*4}A(t)}\right)^{2n^*}\times\exp\left(-\frac{2Z^3}{3n^{*3}A(t)}\right). \tag{15}$$

Here $\omega_a=4.1\times10^{16}$ s^{-1} is the atomic frequency, l is the orbital quantum number, $A(t)$ is the laser field amplitude in atomic units, P is a polarization dependent factor with $P=[3A(t)n^{*3}/\pi Z^3]^{1/2}$ for a linear polarization, Z is the charge of a produced ion, and $n^*=Z(\mathcal{R}/E_i)^{1/2}$ is the effective quantum number for the ground state of an atom (ion) with the ionization potential E_i ($\mathcal{R}=13.6$ eV).

For argon the evolutions of the electron density N_e/N_0 and of the nonlinear refractive index $(n-1)N_{cr}/N_0$, where $N_{cr}=\pi/r_e\lambda^2$ is the critical electron density, are illustrated in Fig. 3 for 5 fs, 25 fs, and 100 fs Ti:sapphire laser pulses ($\lambda=800$ nm). Laser intensity profiles are shown in Figs. 3(a) and 3(c) by thick solid lines. Other lines in Figs. 3(a) and 3(c) demonstrate the evolution of the electron density for different pulse durations and laser intensities (a) $I_1=8\times10^{13}$ W/cm^2 and (c) $I_1=2\times10^{14}$ W/cm^2, respectively.

In calculations of the refractive indices, $n_2=9.8\times10^{-20}$ cm^2/W is used [18]. As can be seen in Fig. 3(b), in a low intensity laser field (weak ionization) the refractive index for the fundamental laser radiation initially grows due to the Kerr effect. This effect is more pronounced for shorter laser pulses. Then, the refractive index decreases due to ionized

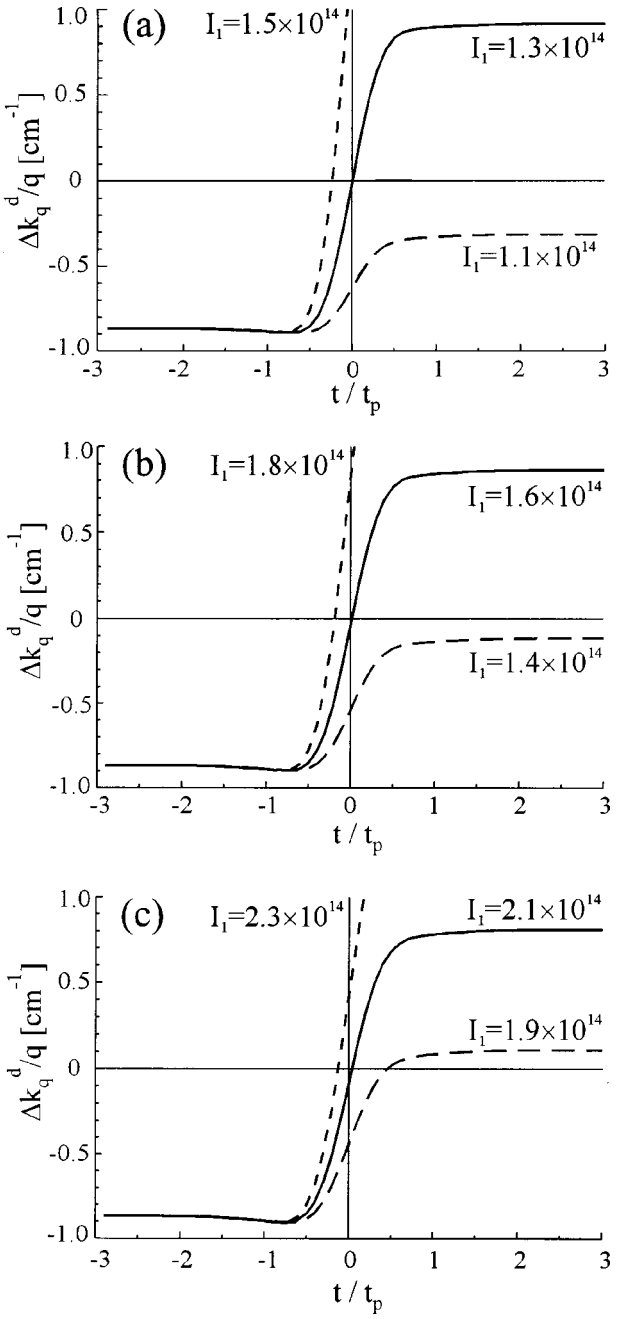

FIG. 4. Evolution of the dispersive wave-vector mismatch in argon at 30 Torr for different laser intensities in W/cm^2 and pulse durations: (a) 100 fs, (b) 25 fs, and (c) 5 fs.

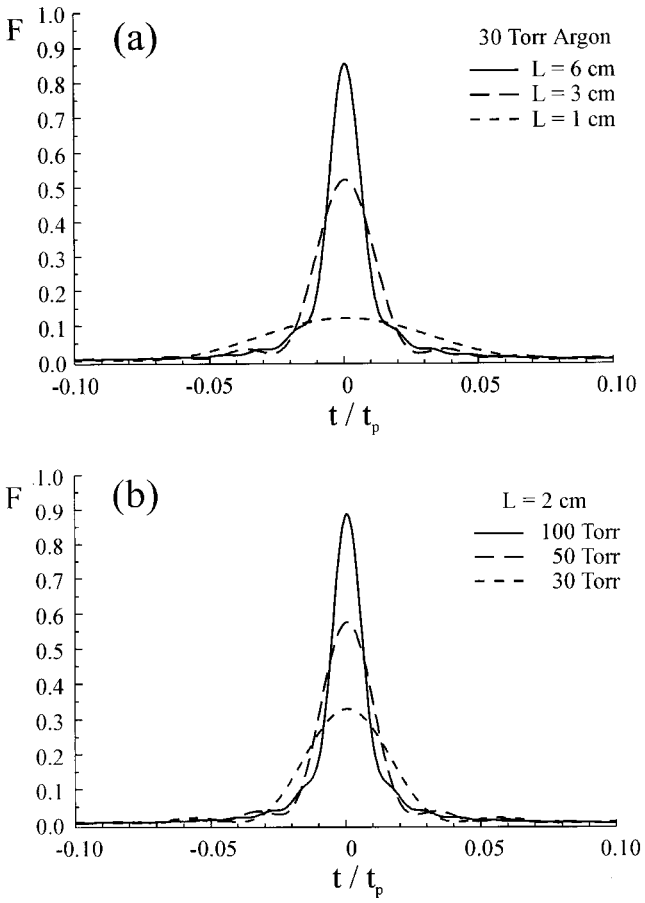

FIG. 5. Temporal behavior of the F factor for the 31st harmonic of Ti:sapphire laser radiation ($\lambda_1=800$ nm) generated in argon. Calculations are performed for (a) different medium lengths and (b) pressures for 25 fs laser pulses with the optimum peak intensity of $I_1=1.6\times10^{14}$ W/cm^2.

electrons. In a high intensity laser field (strong ionization), the influence of the Kerr effect is negligible compared to the negative free electron contribution [see Fig. 3(d)]. In this case the sign of the factor $n-1$ changes during the laser pulse.

For high-order harmonics (far from atomic and ionic resonances) the refractive index n_q is very close to one. Therefore, analogous to the above discussions, at sufficiently high laser intensities there always exists a time moment when the dispersive wave-vector mismatch $\Delta k_q^d=k_q-qk_1=2\pi q(n_q-n_1)/\lambda_1$ becomes equal to zero. Assuming $n_q=1$, in Fig. 4 the evolution of the dispersive wave-vector mismatch $\Delta k_q^d/q$ is shown for different pulse durations and laser intensities. At the beginning, the wave-vector mismatch is negative (due to neutral atoms) and then becomes positive (due to ionized free electrons). The time moment, when Δk_q^d is equal to zero, depends on the laser intensity. In calculations of the conversion efficiency the value of the dispersive phase mismatch at the peak of the laser pulse is important. Assuming $\Delta k_q=\Delta k_q^d$, where Δk_q is the total wave-vector mismatch, it is clear that to get a highest conversion efficiency, the moment of $\Delta k_q^d=0$ should coincide with the peak of the laser pulse (or be close enough). This defines an optimum laser intensity for the high-order harmonic generation. Corresponding intensities are shown in Fig. 4 by solid lines. The optimum intensity is higher for shorter laser pulses due to a lower degree of ionization.

Taking into account the evolution of the dispersive phase mismatch during the laser pulse, we can determine the temporal dependence of the F factor. This dependence is illustrated in Fig. 5 for the 31st harmonic of Ti:sapphire laser radiation ($\lambda_1=800$ nm) generated in argon. Calculations are performed for 25 fs laser pulses with the optimum peak intensity of $I_1=1.6\times10^{14}$ W/cm^2. In Fig. 5(a) the F factor is shown for different medium lengths at a constant gas pres-

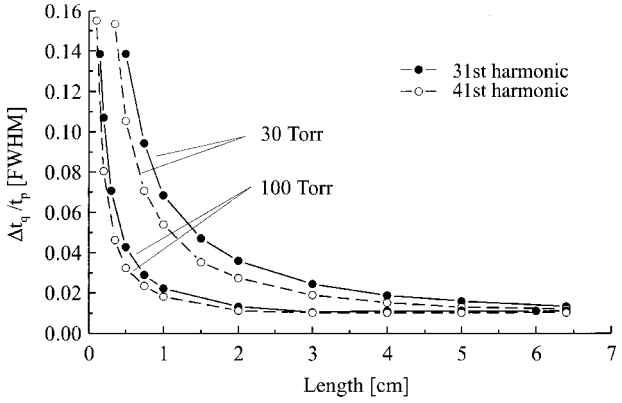

FIG. 6. Temporal pulse widths Δt_q (in units of laser pulse duration t_p) of the 31st and 41st harmonics generated in argon as a function of medium length.

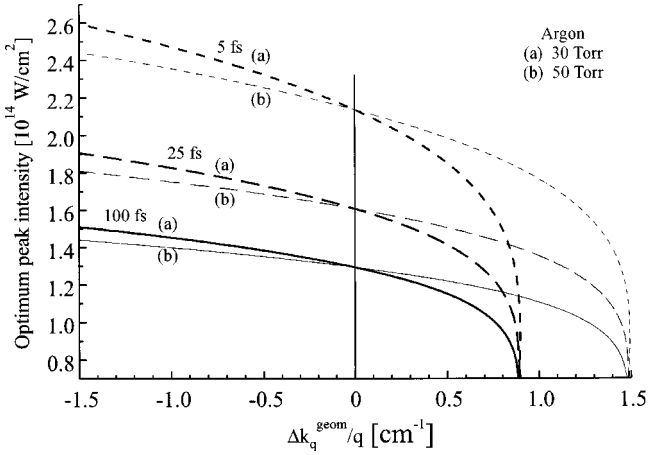

FIG. 7. Optimum peak laser intensity as a function of the geometrical wave-vector mismatch.

sure of 30 Torr. Since the phase-matching condition $\Delta k_q = 0$ is fulfilled only at the peak of the laser pulse, the width of the F factor decreases with the medium length. The same dependence is observed when the gas pressure is increased [see Fig. 5(b)].

At sufficiently high medium length (or gas pressure) the pulse duration of the high-order harmonics is determined by the propagation effects, i.e., by the temporal behavior of the F factor. In Fig. 6 the ratios of the duration of high-order harmonic signal to that of the pump laser pulse are shown for the 31st and 41st harmonics. These values are well below the prediction of the perturbation theory $\Delta t_q / t_p = 1/\sqrt{q}$. As can be seen in Fig. 6, due to the propagation effects the 31st and 41st harmonics become 50 times shorter than the pump laser pulse. This corresponds to the generation of attosecond pulses. Note that the same dependences, demonstrated in Figs. 5 and 6, are obtained when the calculations are repeated for 100 fs and 5 fs pulses with the optimum intensities $I_1 = 1.3\times 10^{14}$ and $I_1 = 2.1\times 10^{14}$ W/cm^2, respectively.

For large optical thicknesses $\tau_q \gg 1$ (or large medium length and/or high gas pressure) the shape of the F factor is determined by $F \simeq 1/\{1+4[\Delta k_q(t)/\alpha_q]^2\}$. This expression defines the limiting temporal width of the F factor and of the high-order harmonics.

IV. GEOMETRICAL OR FIBER PHASE MISMATCH

In the high-order harmonic generation experiments short laser pulses are usually focused into a gas jet (cell) or sent through a gas-filled hollow-core fiber. In these cases the wave-vector mismatch is a sum of a time dependent dispersive mismatch Δk_q^d, considered in the previous section, and of a time independent geometrical mismatch Δk_q^g

$$\Delta k_q = \Delta k_q^d + \Delta k_q^g. \tag{16}$$

For pulses weakly focused into a gas jet the geometrical phase mismatch is given by

$$\Delta k_q^g = 2(q-1)/b > 0, \tag{17}$$

where b is the confocal parameter ($b \gg L$ is assumed). For pulses coupled into a hollow-core fiber [19]

$$\Delta k_q^g = \frac{\lambda_1}{4\pi a^2}(q u_1^2 - u_q^2/q) > 0, \tag{18}$$

where a is the fiber radius, u_1 and u_q are the propagation mode constants for the pump pulse and q-order harmonic, respectively. In both cases the geometrical phase mismatch is positive and has the same dependence on the harmonic order $\Delta k_q^g \sim q$ for $q \gg 1$. Therefore, for phase matching there is no principle difference between gas jets and hollow-core fibers.

In the presence of a time independent geometrical phase mismatch, the phase-matching condition is given by $\Delta k_q^d + \Delta k_q^g = 0$. To satisfy this condition at the peak of the laser pulse, a lower laser intensity is required than in case of $\Delta k_q^g = 0$, since Δk_q^d is negative at the beginning of the laser pulse and Δk_q^g is usually positive. In Fig. 7 dependences of the optimum laser intensity on the geometrical phase mismatch are shown for argon. Calculations are performed for different pulse durations and gas pressures. In the case of a zero geometrical phase mismatch, the phase-matching condition ($\Delta k_q^d = 0$) can be fulfilled for each pulse duration at a certain optimum intensity, independent of the gas pressure. For $\Delta k_q^g \neq 0$ optimum laser intensities are different for different gas pressures (especially for positive Δk_q^g).

The effect of the geometrical phase mismatch on the F factor, which determines the high-order harmonic intensity [see Eq. (6)], is demonstrated in Fig. 8. Calculations are performed for Xe with an absorption cross section for the high-order harmonic $\sigma_q = 7.4$ Mb and a medium length $L = 0.1$ cm. This absorption cross section corresponds to the generation of the ninth harmonic using pump radiation at 400 nm.

As can be seen, due to the geometrical phase mismatch the shape of the F factor becomes asymmetric. Since the dispersive phase mismatch grows with the gas pressure (particle density), the pressure independent parameter $\Delta k_q^d / p$ is

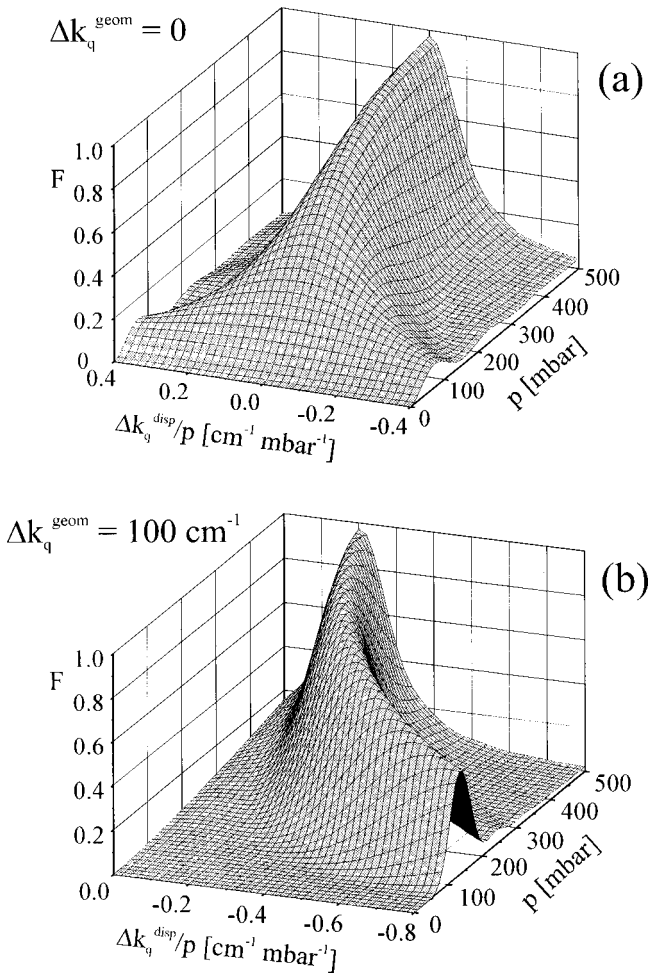

FIG. 8. Illustration of the effect of the geometrical phase mismatch on the F factor (6). Calculations are performed for a 0.1 cm long xenon medium, using $\sigma_q = 7.4$ Mb.

used as one of the axes. For a fixed value of this parameter, Fig. 8 illustrates the variation of the F factor with the gas pressure.

The maximum value of the high-order harmonic signal (and of the F factor), considered as a function of the gas pressure, is not automatically determined by the phase-matching condition $\Delta k_q^d = -\Delta k_q^g$ (or $\delta = 0$). To make this clear, we introduce a density independent parameter $\kappa_q^d = \Delta k_q^d / N$ that allows us to rewrite $\delta = 2\Delta k_q / \alpha_q$ in the form $\delta = 2(\kappa_q^d + \Delta k_q^g / N)/\sigma_q$. The phase matching occurs (when κ_q^d is negative) at the particle density $N_{pm} = \Delta k_q^g / |\kappa_q^d|$. At this density the F factor given by Eq. (6) reduces to $F = F_{pm} = [1 - \exp(-\tau_q^{pm}/2)]^2$, where $\tau_q^{pm} = N_{pm}\sigma_q L$.

Another limiting case is realized at very high particle densities $N \to \infty$, where $\delta \to \delta_\infty = 2\kappa_q^d/\sigma_q$ and $F \to F_\infty = 1/(1 + \delta_\infty^2)$. It is clear that when F_{pm} is smaller than F_∞, the maximum value of the F factor is reached at higher particle densities $N > N_{pm}$. To have a maximum at $N = N_{pm}$, the condition $\tau_q^{pm} \gg 2$ or $\Delta k_q^g \sigma_q L / |\kappa_q^d| \gg 2$ should be fulfilled. In this case $F_{pm} \simeq 1$, whereas $F_\infty < 1$. In practice, as our calculations show, $\tau_q^{pm} \geqslant 4$ is already enough to ensure that the maximum value of the F factor is reached very close to $N = N_{pm}$. At fixed values of σ_q and κ_q^d, one can fulfill this condition by increasing the geometrical phase mismatch or the medium length.

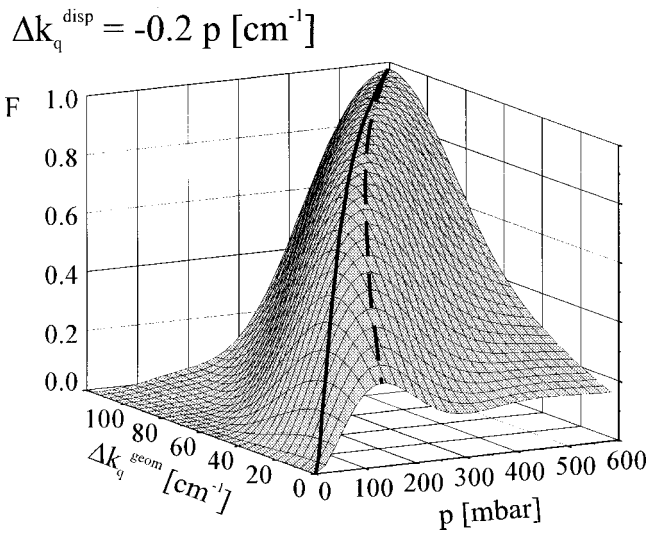

FIG. 9. Dependence of the F factor on the geometrical phase mismatch and gas pressure ($\sigma_q = 7.4$ Mb and $L = 0.1$ cm). The thick solid line corresponds to $\Delta k_q^{geom} + \Delta k_q^{disp} = 0$. Maximum values of the F factor are shown by the dashed line.

An illustration to the above discussion is given in Fig. 9. In this figure the behavior of the F factor as a function of the geometrical phase mismatch and gas pressure is shown for $\sigma_q = 7.4$ Mb and medium length $L = 0.1$ cm. The phase-matching condition is fulfilled along the thick solid line. Maximum values of the F factor are reached along the dashed line. As can be seen, for small Δk_q^g the phase-matching condition is realized at low pressures, before the maximum of the F factor is reached. With the growth of the geometrical phase mismatch both curves approach each other.

Concluding this section we note that the geometrical effects can be included into the dispersive phase mismatch. This can be done by introducing a geometrical correction to the refractive index $n^g = -\lambda/\pi b$ for a gas jet and $n^g = -\lambda^2 u^2 / 8\pi^2 a^2$ for a fiber. Adding this term to the right hand side of Eq. (9), the total wave-vector mismatch can be written as $\Delta k_q = 2\pi q (n_q' - n_1')/\lambda_1$, where $n' = n + n^g$ are the modified refractive indices.

V. ATTENUATION OF THE PUMP WAVE

In theoretical modelling of high-order harmonic generation, any changes of the pump wave intensity during propagation in a nonlinear medium are usually neglected. This assumption seems very reasonable, since the pump intensity is much higher than the intensity of the generated radiation. Here we demonstrate that this is not generally true. Even small changes in the pump wave intensity can have a dramatic effect on the high-order harmonic generation efficiency.

Changes of the pump wave intensity inside a gaseous medium occur due to scattering, various self-action effects, and

multiphoton absorption. In hollow-core fibers the pump losses are due to the energy transfer into nonguiding spatial modes. To take all these effects into account we introduce an attenuation coefficient α_1 for the pump intensity (on the beam axis) $I_1 = I_{10}\exp(-\alpha_1 z)$, where I_{10} is the boundary value.

The general dependence of the nonlinear dipole moment on the pump field is given by $d_q^{NL} \sim A_1^p$, where the exponent p can be arbitrary $p \leqslant q$. In our discussions below, the actual value of the exponent p is not of principle importance. Without a lack of generality we can assume $p = q$ and $d_q^{NL} = d_{q0}^{NL}\exp(-q\alpha_1 z/2)$, where the value of d_{q0}^{NL} is calculated at the medium boundary ($z = 0$). For $p \neq q$ the same result will be obtained when α_1 is replaced by $\alpha_{1p} = q\alpha_1/p$.

Solving Eq. (2) taking into account the attenuation of the pump wave, we obtained a modified expression for the intensity of the q-order harmonic

$$I_q = \frac{\pi\omega_q^2}{2cn_q}|d_{q0}^{NL}|^2 N^2 L^2 \exp[-(q\alpha_1 + \alpha_q)L/2] \times \frac{\sin^2(\Delta k_q L/2) + \sinh^2[(q\alpha_1 - \alpha_q)L/4]}{(\Delta k_q L/2)^2 + [(q\alpha_1 - \alpha_q)L/4]^2} \tag{19}$$

$$= \frac{2\pi\omega_q^2}{cn_q}\frac{|d_{q0}^{NL}|^2}{\sigma_q^2}F \tag{20}$$

with a new form factor given by

$$F = \frac{4}{(\eta-1)^2 + \delta^2}\exp[-\tau_q(\eta+1)/2] \times \{\sin^2(\delta\tau_q/4) + \sinh^2[\tau_q(\eta-1)/4]\}$$

$$= \frac{1}{(\eta-1)^2 + \delta^2}\{\exp(-\tau_q\eta) + \exp(-\tau_q) - 2\cos(\delta\tau_q/2)\exp[-\tau_q(\eta+1)/2)]\}. \tag{21}$$

Here $\eta = q\alpha_1/\alpha_q$ is the attenuation parameter. Other notations are the same as in Eq. (6). For large attenuation parameters $\eta \gg 1$, $F \simeq \exp(-\tau_q)/(\eta^2 + \delta^2) \to 0$.

Due to the attenuation of the pump laser radiation, the maximum value of the F factor (21), considered as a function of the gas pressure, can be reached at lower pressures, before the phase-matching condition $\delta = 0$, giving $F_{pm} = [\exp(-\tau_q\eta/2) - \exp(-\tau_q/2)]^2/(\eta-1)^2$, is realized.

In Fig. 10 dependences of the F factor on δ and η are demonstrated for (a) $\tau_q = 1$ and (b) $\tau_q = 3$. It can be clearly seen that the growth of the attenuation parameter η results in a rapid decrease of the F factor and conversion efficiency.

Propagation of short laser pulses in gaseous media can be accompanied by self-focusing and self-guiding effects due to a positive nonlinear refractive index coefficient $n_2 > 0$. For a self-focusing laser pulse the field amplitude on the beam axis grows with the medium length. In this case the attenuation coefficient α_1 is negative. What happens for the negative attenuation coefficient is illustrated in Fig. 10. As can be

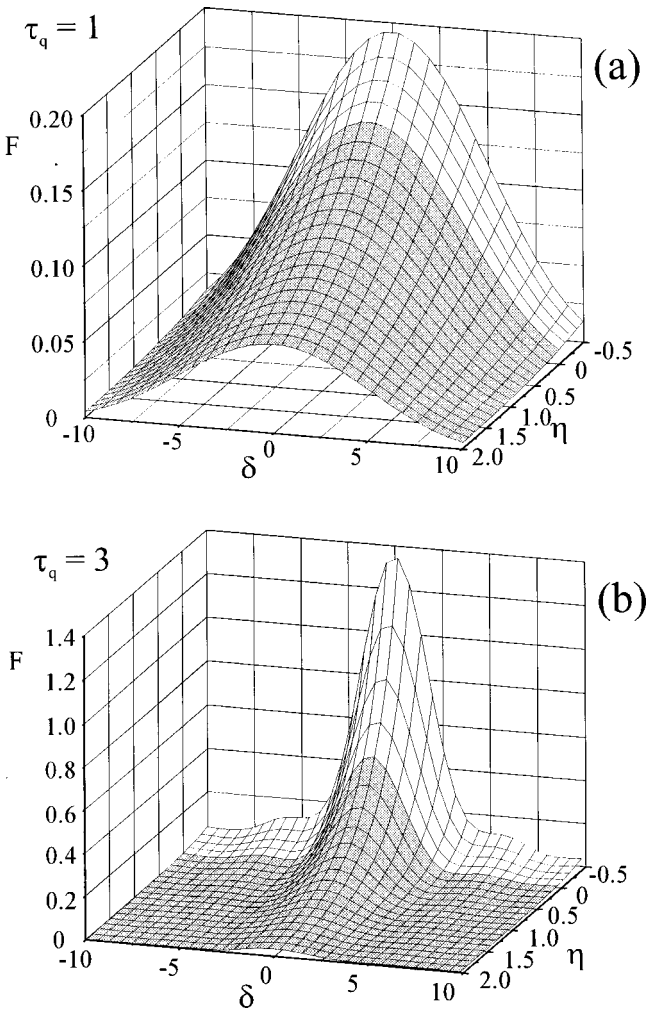

FIG. 10. Dependences of the F factor (21) on $\delta = 2\Delta k_q/\alpha_q$ and on the attenuation parameter $\eta = q\alpha_1/\alpha_q$ for different optical thicknesses (a) $\tau_q = 1$ and (b) $\tau_q = 3$.

seen, for the self-focusing laser pulse the maximum value of the F factor can be larger than 1. This regime is very attractive from the point of conversion efficiency. Very efficient high-order harmonic generation can be expected when, due to the self-focusing, the pump laser intensity initially grows inside the medium up to the optimum value (giving $\Delta k_q = 0$ at the peak of the laser pulse), and then a self-channeled propagation of the laser pulse with negligible losses occurs. This regime can be easier realized with ultrashort laser pulses allowing us to obtain higher intensities without an onset of medium ionization.

Before turning to a discussion of experimental results, we outline here the limits of the above presented approximate model for high-order harmonic generation. In this model the radial dependence of the field intensity, in a plane normal to the beam axis, is neglected. The value of the dispersive phase mismatch is calculated at the peak of the laser pulse. To reproduce experimental data the attenuation cross section for the pump wave is considered as a fit parameter. Applying the above model for ultrashort laser pulses with only a few optical cycles one should take into account higher-order terms of the dispersion theory and be careful with the slowly

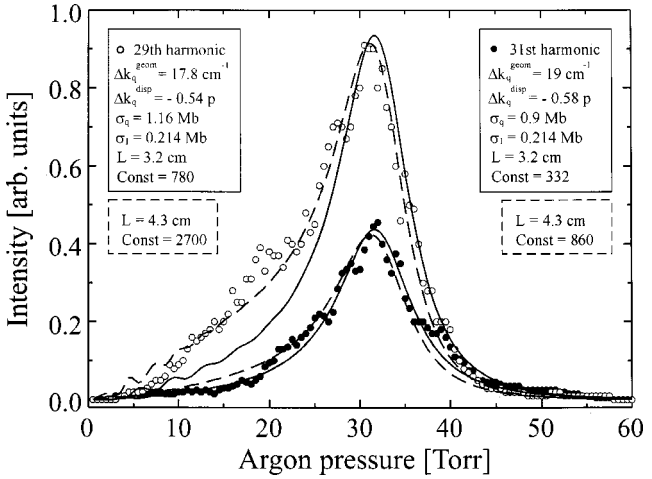

FIG. 11. Signals of the 29th and 31st harmonics observed in [8] as a function of argon gas pressure. Results of our calculations are shown by solid lines for a medium length of $L=3.2$ cm and by dashed lines for $L=4.3$ cm.

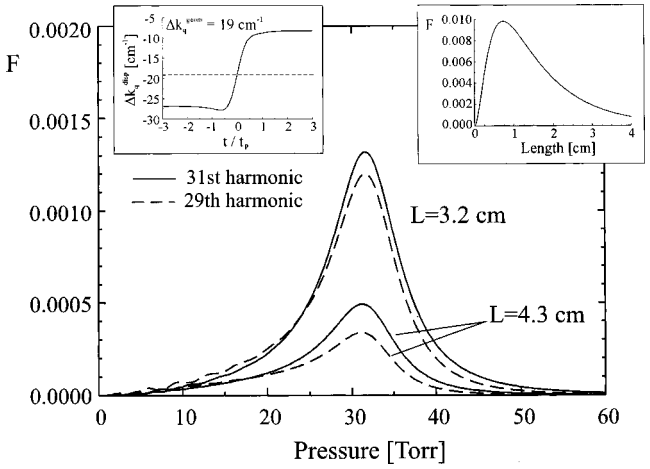

FIG. 12. F factors for the 29th and 31st harmonics observed in [8]. In the left insert the temporal behavior of the dispersive phase mismatch for the 31st harmonic at 30 torr argon pressure is illustrated. The variation of the F factor with the medium length at this pressure is shown in the right inset.

varying envelope approximation which can lose its validity [20]. In a high-intensity laser field the tunneling theory (Eq. 15) slightly overestimate the ionization rate. In this case one should take into accout corrections due to above barrier ionization [21].

VI. RECENT EXPERIMENTS

Here we give a brief review of experimental results obtained by other groups. In [8] phase-matched high-order harmonic generation in argon-filled hollow-core fibers was demonstrated. Using Ti:sapphire pump laser pulses at 800 nm, the 29th and 31st harmonics with an estimated conversion efficiency of 10^{-6} to 10^{-5} were generated. The 29th and 31st harmonic signals observed in [8] as a function of gas pressure are shown in Fig. 11 by empty and filled circles. Using Eq. (21) for the F factor (multiplied by a constant) and the attenuation cross section for the pump wave σ_1 as a fit parameter, we obtain results shown in Fig. 11 by the solid (for the medium length $L=3.2$ cm) and dashed ($L=4.3$ cm) lines. Calculations are performed for two medium lengths since in [8] there is some uncertainty with its actual value. Other parameters used in calculations are shown in inserts in Fig. 11 and correspond to the experimental data [8]. The geometrical phase mismatch is determined by Eq. (18) with $u_1=2.4$, neglecting the high-order harmonic contribution. The dispersive phase mismatch is calculated at the peak of the laser pulse (1.4×10^{14} W/cm^2) assuming $n_q=1$. Absorption cross sections for the high-order harmonics are taken from [15].

It is important that only taking into account the attenuation of the pump wave we are able to reproduce the experimental observations. The attenuation cross section $\sigma_1=0.214\times10^{-18}$ cm^2 corresponds approximately to 50% intensity losses at the fiber output, which seems very reasonable. In the left insert in Fig. 12 the temporal behavior of the dispersive phase mismatch for the 31st harmonic at 30 torr argon pressure is illustrated. As can be seen, the phase-matching condition $\Delta k_q^d+\Delta k_q^g=0$ is really fulfilled at the peak of the laser pulse. In spite of this, the value of the F factor calculated using Eq. (21) is much smaller than 1 (see Fig. 12). This demonstrates that the phase matching alone is not able to provide a high conversion efficiency. It is also important to minimize losses of the pump wave intensity. The variation of the F factor with the medium length at 30 torr is shown in the right insert. For a 1 cm long fiber our calculations predict five times higher conversion efficiency than it was observed with the 3 cm long fiber in [8].

In [9] high-order harmonic generation in a gas jet and in a gas injected into a hollow-core fiber were compared. In these experiments only the gas backing pressure was given. Therefore, to find the actual gas pressure p_a we have to introduce a correction factor a giving $p_a=p/a$, where p is the backing pressure. This factor enters in Eq. (21) as an additional fit parameter. In Fig. 13 experimental results [9] and our fits for the 15th harmonic of Ti:sapphire laser radiation are shown. Laser intensities and other parameters used in calculations are given in inserts. Values of the dispersive phase mismatch are calculated at the peak of the laser pulse using for the refractive indices $n_q\simeq1-2\times10^{-4}$ (xenon) and $n_q\simeq1-10^{-4}$ (argon) taken at atmospheric pressure. For xenon $n_2=8.1\times10^{-19}$ [18] is used. As can be seen in Fig. 13, experimental results [9] can be very good reproduced by Eq. (21). From our calculations it follows that at the peak of the laser pulse phase-matching condition was not realized in xenon. In this case phase matching was reached earlier in time at lower intensities. For argon the phase-matching condition was fulfilled at 110 mbar backing pressure. The observed signal for argon was lower due to a larger absorption cross section for the 15th harmonic and smaller polarizability.

VII. EXPERIMENTAL SETUP AND DISCUSSIONS

In our investigations of high-order harmonic generation and frequency mixing in gaseous media, a 150 fs Ti:sapphire

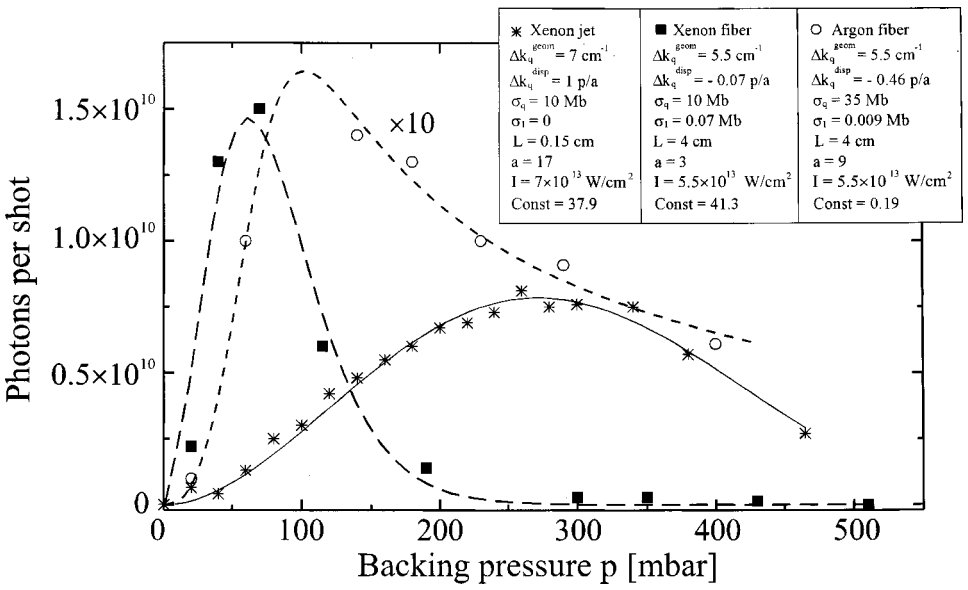

FIG. 13. Experimental results [9] and our fits for the 15th harmonic of Ti:sapphire laser radiation.

laser system (BMI Alpa 10A) operating at 790 nm is used. To perform two-color mixing experiments the laser radiation is frequency doubled in a 2 mm potassium dihydrogen phosphate (KDP) crystal. The typical experimental setup is shown in Fig. 14. The fundamental is separated from the second harmonic by a beam splitter. Owing to a variable delay the fundamental and the second harmonic can be recombined. Each of the beams is focused with an $f=1000$ mm lens into the nonlinear medium. Pulse energies in our experiments can be varied in the range of $\leqslant 50$ mJ for the fundamental and $\leqslant 25$ mJ for the second harmonic, respectively.

As nonlinear media gas jets injected by one of two pulsed nozzles are used. One nozzle has a single output hole with a diameter of 1 mm. Another nozzle has five output slits with a width of 0.2 mm and lengths ranging from 1 mm to 5 mm. By moving this nozzle perpendicular to the laser-beam axis one can vary the interaction length.

Below we present results of three experiments performed with xenon using different laser parameters and medium lengths. High-order harmonics are generated by fundamental radiation (ω), second harmonic (2ω), and two-color $(\omega,2\omega)$ laser radiation. Adding the second harmonic to the fundamental laser radiation allows for an increase in the high-order harmonic generation efficiency. This enhancement appears due to a growth of the nonlinear atomic dipole moment and due to additional possibilities for a better phase matching.

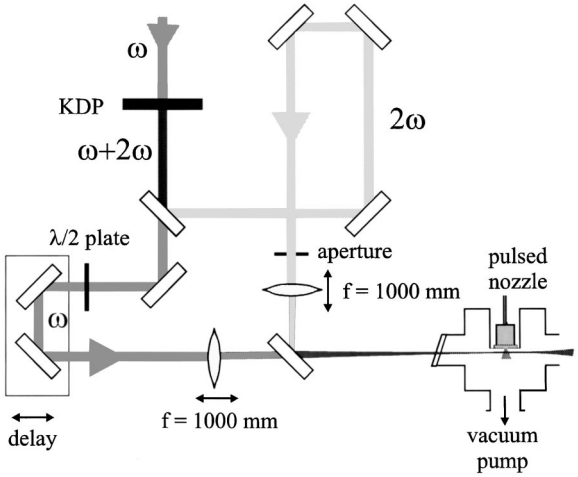

FIG. 14. Experimental setup.

First experiment. These results are obtained at approximately the same intensities of the fundamental and second harmonic radiation of 4×10^{13} W/cm^2 for a 5 mm long medium length. In Fig. 15(a) the signals of the nine-order harmonic generated in xenon by fundamental (ω) and two color $(\omega,2\omega)$ laser radiation are shown as a function of the gas backing pressure. The confocal parameter for the fundamental laser radiation is in the range of $b\simeq 5\div 6$ mm. This corresponds for the ninth harmonic generated by the fundamental radiation alone to a geometrical phase mismatch of approximately 30 cm^{-1}. The calculated value of the dispersive phase mismatch at the peak of the laser pulse is $\Delta k_q^d = -0.8p_a$, where $p_a=p/a$ is the actual pressure inside the gas jet and p is the backing pressure. In calculations of the temporal evolution of the refractive index for the ninth harmonic n_2 effects (like cross phase modulation) are neglected and $n_q\simeq 1-10^{-3}$ (at atmospheric pressure) is used as a starting value. The absorption cross section for the ninth harmonic is $\sigma_q\simeq 22$ Mb [15]. Using $\sigma_1=0$ and $a=15$ as fit parameters for the ninth harmonic generated by the fundamental radiation alone, the dashed curve in Fig. 15(a) is obtained. Keeping these parameters unchanged, we can reproduce results of the two-color experiment by slightly varying the values of the geometrical and dispersive phase mismatch. This is a legitimate procedure since it is reasonable to expect that both values will be modified in the presence of the second field. There are several reasons for this modification: in a two-color laser field harmonics can be generated by different mixing processes; there exists always some uncertainty in the spatial and temporal overlap between the two pulses;

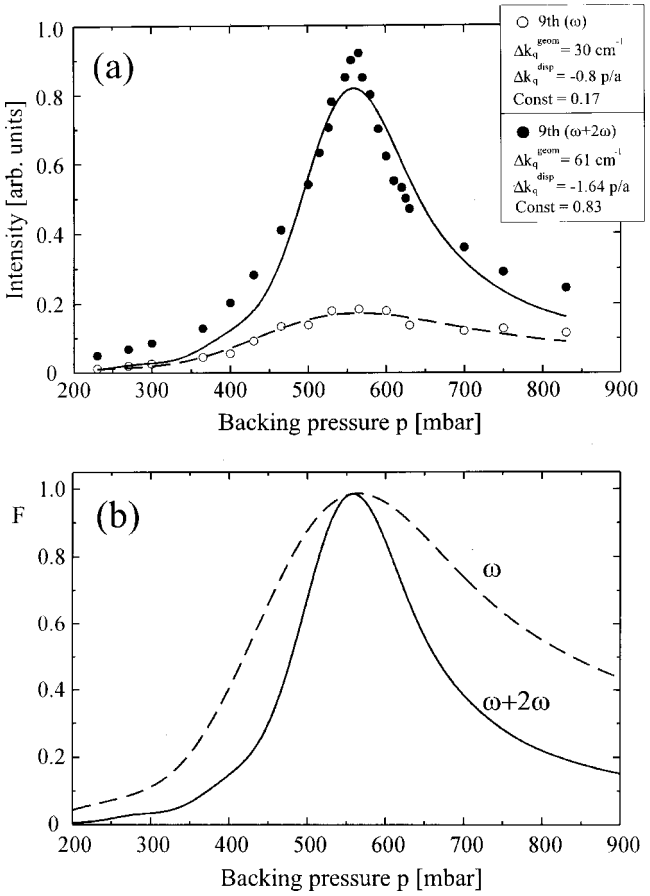

FIG. 15. First experiment. Signals of the ninth harmonic as a function of the xenon backing pressure generated by fundamental (ω) and two-color laser radiation ($\omega, 2\omega$) in (a) a 5 mm long medium and (b) corresponding values of the F factor. Parameters used in calculations are $\sigma_q = 22$ Mb, $\sigma_1 = 0$, $a = 15$, and given in the insets.

the second pulse changes refractive index for the fundamental wave due to cross phase modulation and ionization (and vice versa). The attenuation cross section $\sigma_1(\omega)$ can also be modified by the second pulse (especially when this pulse arrives earlier in time). Moreover, the attenuation of the second harmonic itself, $\sigma_1(2\omega) \neq 0$, can become important.

Data given in inserts in Fig. 15(a) show that the phase-matched generation of the ninth harmonic by ω and $\omega + 2\omega$ fields occurs in both cases at the same backing pressure of 560 mbar. At this pressure, as can be seen in Fig. 15(b), the F factor (21) reaches its maximum value $F \simeq 1$. The fact that the ninth harmonic signal is stronger in the two-color field can be explained by a reduced order of the required nonlinearity and by a higher atomic polarizability. These results are analogous to that obtained in [4], where phase-matched high-order harmonic generation by a two-color laser field has been demonstrated for the first time.

Second experiment. This experiment is performed with a 1.5 mm medium length. To get a higher particle density, the laser pulses were focused very close to the nozzle output. Estimated intensities of the fundametal and second harmonic are 4×10^{13} and 5×10^{13} W/cm^2, respectively. The confocal parameter for the fundamental was left unchanged $b \simeq 5 \div 6$ mm, whereas for the second harmonic the confocal parameter was increased up to $b \simeq 2$ cm by an apperture.

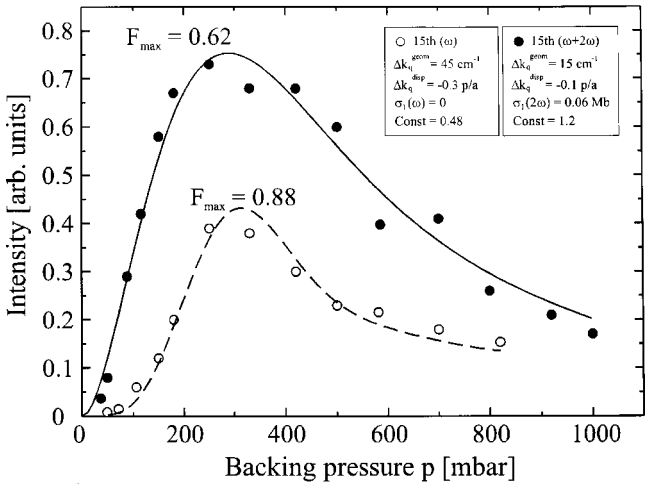

FIG. 16. Second experiment. Generation of the 15th harmonic by single frequency and two-color laser fields in a 1.5 mm long xenon medium. Maximum values of the F factor (21) (F_{max}) are shown. Parameters used in calculcations are $\sigma_q = 10$ Mb and $a = 2$.

In Fig. 16 the generation of the 15th harmonic by single frequency and two-color laser fields is illustrated. In calculations, for the 15th harmonic the absorption cross section $\sigma_q = 10$ Mb and the refractive index $n_q \simeq 1 - 2 \times 10^{-4}$ (at atmospheric pressure) are used. Using experimental values for the geometrical and dispersive phase mismatch, the signal of the 15th harmonic generated by the fundamental radiation alone is calculated. As fit parameters $\sigma_1 = 0$ and $a = 2$ are used. Results of the two-color experiments are reproduced with the parameters shown in insert. As can be seen, in addition to Δk_q^g and Δk_q^d the attenuation cross section should also be modified in this case. We relate this to the attenuation of the second harmonic $\sigma_1(2\omega) = 0.06$ Mb (this assumption is proved in the next figure). Phase-matched generation of the 15th harmonic occurs at the backing pressure of 300 mbar. The maximum values of the F factor are given in the figure.

In Fig. 17(a) signals of the seventh and ninth harmonics generated by the second harmonic radiation alone are shown. These results are reproduced without any fit parameters, using $a = 2$ and $\sigma_1(2\omega) = 0.06$ Mb obtained before. The values of the dispersive phase mismatch are calculated at the peak of the laser pulse with $n_{q=7} \simeq 1 - 3 \times 10^{-4}$ and $n_{q=9} \simeq 1 - 2 \times 10^{-4}$ taken at atmospheric pressure. All parameters are shown in inserts. As follows from our calculations, phase matching for the seventh and ninth harmonics is fulfilled at 46 and 76 mbar, respectively. The signals continue to grow and have their maxima at higher pressures, since the total value of the mismatch is not large. Corresponding values of the F factor (at curve maximum) are given in the figure.

Phase matching in a two-color field is not automatically better than in a single frequency case. In Fig. 17(b) the generation of 13th harmonic by ω and $\omega + 2\omega$ laser fields is shown. The signal of the 13th harmonic generated by the fundamental alone is calculated without any fit parameters (with $a = 2$ and $\sigma_1 = 0$). Dispersive phase mismatch is deter-

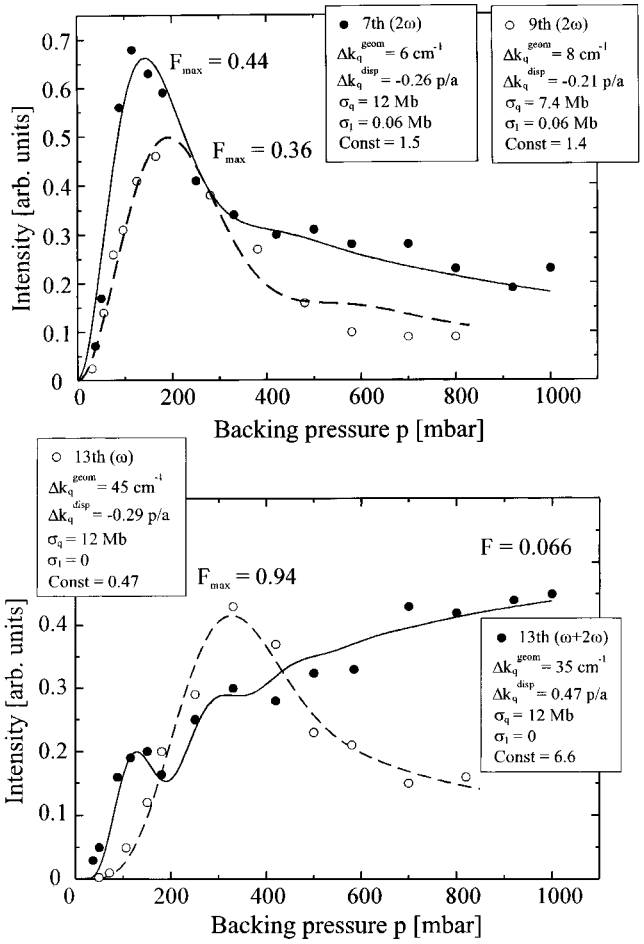

FIG. 17. Second experiment (xenon, $L=1.5$ mm, $a=2$). (a) Signals of the seventh and ninth harmonics generated by second harmonic radiation and (b) signals of the 13th harmonic generated by fundamental (ω) and two-color ($\omega,2\omega$) laser radiation.

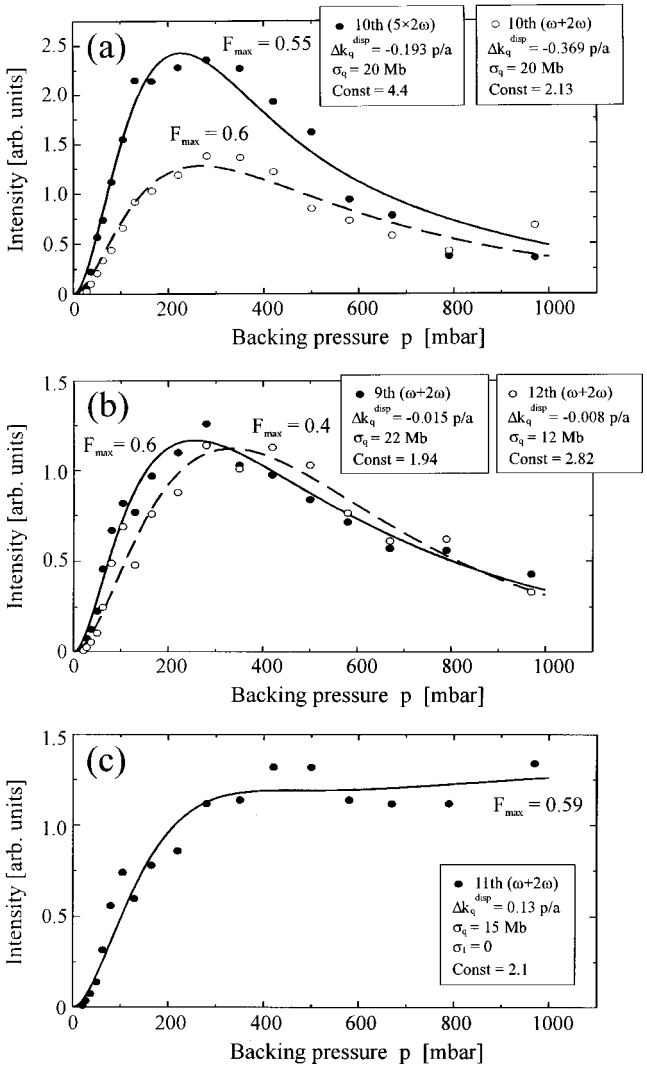

FIG. 18. Third experiment (xenon, $L=4$ mm, $\Delta k_q^g=2$ cm^{-1}, $a=10$, $\sigma_1=0.4$ Mb). (a) Signals of the fifth harmonic generated by 2ω and $\omega+2\omega$ laser radiation and signals of (b) 9th and 12th harmonics and (c) 11th harmonic generated by two-color laser radiation.

mined at the peak of the laser pulse with $n_q \simeq 1-3\times10^{-4}$. To reproduce results of the two-color experiment, parameters shown in right insert in Fig. 17(b) are used. As can be seen, in the $\omega+2\omega$ laser field phase-matching condition is not fulfilled. In spite of that, in this case the F factor is much smaller, the observed 13th harmonic signals have compared intensities. This can be explained by a larger nonlinear atomic dipole moment produced by $\omega+2\omega$ field.

Third experiment. This experiment is performed with a 4 mm medium length. The intensity and the confocal parameter for the fundamental is left unchanged. For the second harmonic the confocal parameter $b\simeq4$ cm is used and the intensity is increased to 6×10^{13} W/cm^2.

The signals of the fifth harmonic generated by the 2ω and $\omega+2\omega$ laser radiation are shown in Fig. 18(a). The value of the geometrical phase mismatch for this harmonic is $\Delta k_q^g=2$ cm^{-1}. In calculations of the dispersive phase mismatch for the fifth harmonic the value $n_q\simeq1-5\times10^{-4}$ is used. Below we keep the value of the geometrical phase mismatch the same for all neighbor harmonics. The fit parameters $a=10$ and $\sigma_1=0.4$ Mb allow for reproduced experimental results for all harmonics shown in Figs. 18(a) and 18(b). The relatively large attenuation cross section for the second harmonic, compared to the previous experiment, can be explained by a stronger defocusing. By way of exception, the signal of the 11th harmonic shown in Fig. 18(c) can only be reproduced assuming $\sigma_1=0$.

In the last experiment the generation of all harmonics is not phase matched. This is a result of not optimum (very high) second harmonic intensity. A very small geometrical phase mismatch is also disadvantageous. In this case propagation effects are not able to suppress harmonics generated without a perfect phase matching.

Concluding this section we emphasize that, only taking into account all factors limiting the high-order harmonic generation efficiency (pump losses, harmonic absorption, geometrical and dispersive phase mismatch), we are able to obtain a very good agreement between calculations and experimental results.

VIII. PARAMETRIC GENERATORS AND AMPLIFIERS

The highest conversion efficiency that has been obtained so far for the 15th harmonic generated in xenon is 4×10^{-5} [9]. Here we analyze theoretical possibilities promising to improve this efficiency further. We hope that this can be done by the development of high-order parametric amplifiers (HOPA's), which has been recently suggested in [22]. HOPA's can be used as efficient generators of XUV radiation and as amplifiers of high-order harmonic signals. In contrast to the current x-ray lasers having very narrow amplification bandwidth, broadband HOPA's will be able to amplify femto- and attosecond pulses.

In HOPA's, signal (ω_s) and idler (ω_i) waves are generated as a result of the multiphoton process $q\omega_p=\omega_s+\omega_i$, where ω_p is the pump-laser frequency and $\omega_s\geqslant\omega_i$. The idler frequency is arbitrary and can be in the visible, vacuum ultraviolet (VUV) or XUV spectral range. In our previous publication [22] we have presented some new ideas on HOPA's and provided simple theoretical descriptions assuming, for example, that the medium is transparent for the generated fields. Here we consider high-order parametric amplification in absorbing media.

We start from an idealized case, when there is only one process $q\omega_p=\omega_s+\omega_i$ responsible for the generation of the signal and idler waves. For weak generated and strong pump fields this process can be described by the following equations that commonly appear in nonlinear optics [23]

$$\frac{dA_i}{dz}+\frac{\alpha_i}{2}A_i=i\Gamma_i\exp[-i\Delta kz],$$
$$\frac{dA_s}{dz}+\frac{\alpha_s}{2}A_s=i\Gamma_s\exp[-i\Delta kz], \tag{22}$$

where A_j and α_j are the field amplitudes and absorption coefficients, $\Delta k=k_s+k_i-qk_p$ is the wave-vector mismatch, and

$$\Gamma_i=\frac{2\pi\omega_i}{cn_i}Nd^{NL}(\omega_i),\quad \Gamma_s=\frac{2\pi\omega_s}{cn_s}Nd^{NL}(\omega_s). \tag{23}$$

In these expressions N is the atomic density, n_j are the refractive indices, $d^{NL}(\omega_i)=X(\omega_i)A_s^*$ and $d^{NL}(\omega_s)=X(\omega_s)A_i^*$ are the amplitudes of the nonlinear atomic dipole moments oscillating at the frequencies ω_i and ω_s, respectively. $X(\omega_i)$ and $X(\omega_s)$ are the cross polarizabilities relating the induced dipole moments with the signal and idler fields. In perturbation theory

$$X(\omega_{s,i})=\frac{(q+1)\chi^{(q+1)}(\omega_{s,i})}{2^q}A_p^q, \tag{24}$$

where $\chi^{(q+1)}(\omega_{s,i})$ are the nonlinear atomic susceptibilities. Sufficiently far from the resonances the cross polarizabilities $X(\omega_{s,i})=X$ are equal.

Using A_{i0} and A_{s0} as boundary values (at $z=0$) for the field amplitudes and introducing new notations for the nonlinear coupling coefficients between the idler and signal waves

$$\gamma_{s,i}=\frac{2\pi\omega_{s,i}}{cn_{s,i}}NX, \tag{25}$$

the general solution of the system of Eqs. (22) can be obtained

$$A_i^*=\left\{-i\frac{\gamma_i^*}{G}A_{s0}\sinh(Gz)+A_{i0}^*\left[\cosh(Gz)+\frac{\beta}{G}\sinh(Gz)\right]\right\}\exp\left(-\frac{\alpha_i}{2}z-\beta z\right),$$
$$A_s=\left\{i\frac{\gamma_s}{G}A_{i0}^*\sinh(Gz)+A_{s0}\left[\cosh(Gz)-\frac{\beta}{G}\sinh(Gz)\right]\right\}\times\exp\left(-\frac{\alpha_s}{2}z+\beta z\right), \tag{26}$$

where $G=\sqrt{\beta^2+\gamma^2}$ and

$$\beta=\frac{1}{2}\left(\frac{\alpha_s-\alpha_i}{2}-i\Delta k\right),$$
$$\gamma=(\gamma_i^*\,\gamma_s)^{1/2}=\frac{2\pi}{c}\left[\frac{\omega_i\omega_s}{n_in_s}\right]^{1/2}N|X|. \tag{27}$$

Here we assume that ω_i is in the visible (or infrared) range, so that $\omega_s\gg\omega_i$ is valid. In inert gases the absorption coefficient for weak visible (or infrared) radiation is equal to zero, $\alpha_i=0$. The phase-matching condition for the process $q\omega_p=\omega_s+\omega_i$ is satisfied when at the peak of the pump laser pulse $q\omega_p(n_p-n_s)=\omega_i(n_i-n_s)$ is fulfilled for the time dependent refractive indices. Assuming $\Delta k=0$, we obtain for large propagation distances $z\gg1/G$

$$A_i^*\simeq\left(-i\frac{2\gamma_i^*}{\alpha_sg}A_{s0}+\frac{g+1}{2g}A_{i0}^*\right)\exp[\alpha_s(g-1)z/4],$$
$$A_s\simeq\left(i\frac{2\gamma_s}{\alpha_sg}A_{i0}^*+\frac{g-1}{2g}A_{s0}\right)\exp[\alpha_s(g-1)z/4], \tag{28}$$

where $g=\sqrt{1+(4\gamma/\alpha_s)^2}>1$ and $G=\alpha_sg/4$. As can be seen from these expressions, the field amplitudes grow exponentially with the medium length. The growth rate depends on the strength of the nonlinear coupling coefficient γ. For a weak coupling between the idler and signal waves $\gamma\ll\alpha_s/4$, we have

$$A_i^*\simeq\left(-i\frac{2\gamma_i^*}{\alpha_s}A_{s0}+A_{i0}^*\right)\exp(2\gamma^2z/\alpha_s),$$

$$A_s \simeq \left(i\frac{2\gamma_s}{\alpha_s}A_{i0}^* + 4\frac{\gamma^2}{\alpha_s^2}A_{s0} \right) \exp(2\gamma^2 z/\alpha_s) = i\frac{2\gamma_s}{\alpha_s}A_i^* . \tag{29}$$

Assuming $A_{s0}=0$, we get for the signal intensity

$$I_s = \frac{cn_s|\gamma_s|^2}{2\pi\alpha_s^2}|A_{i0}|^2 \exp(4\gamma^2 z/\alpha_s)$$

$$= \frac{2\pi\omega_s^2}{cn_s}\frac{|d_0^{NL}(\omega_s)|^2}{\sigma_s^2}\exp(4\gamma^2 z/\alpha_s), \tag{30}$$

where $d_0^{NL}(\omega_s)=XA_{i0}^*$ and σ_s is the absorption cross section. This expression is equivalent to Eq. (5) for the intensity of the q-order harmonic with the F factor replaced by an exponent. In Eq. (30) the parametric gain coefficient is given by

$$\alpha_p = 4\gamma^2/\alpha_s = \frac{2\pi\omega_s\omega_i}{cn_s}\frac{|d_0^{NL}(\omega_s)|^2}{I_{i0}\sigma_s}N, \tag{31}$$

where I_{i0} is the idler intensity.

Here we calculate the value of the gain coefficient in helium for the following parametric process $\omega_s=6\omega_p-\omega_i$. In calculations 25 fs pulses at the third harmonic of the Ti:sapphire laser radiation are used as a pump, $\omega_p=3\omega$ ($\omega=1.55$ eV), and radiation at $\omega_i=\omega/2$ is taken as an idler. This process is very attractive from the point of phase matching (see [22]). For the pump intensity $I_p=5\times10^{14}$ W/cm^2 and the idler intensity $I_{i0}=10^{11}$ W/cm^2, the value of the nonlinear atomic dipole moment $|d^{NL}(\omega_s)|=3.2\times10^{-3}$ (in atomic units) is calculated by solving numerically the time-dependent Schrödinger equation [14]. The absorption cross section $\sigma_s=6.4$ Mb for the signal wave at $\omega_s=17.5\times\omega$ is taken from [15]. Using these data we obtain for the coupling coefficient $\gamma\simeq4\times10^{-19}\ N\ [\mathrm{cm}^{-1}]=\alpha_s/16$ and for the parametric gain coefficient $\alpha_p\simeq10^{-19}\ N\ [\mathrm{cm}^{-1}]$, where N is the particle density in cm^{-3}. At atmospheric pressure $\alpha_p=2.4\ \mathrm{cm}^{-1}$.

In the opposite case of a very strong coupling $\gamma\gg\alpha_s/4$, which is more difficult to realize, we obtain

$$A_i^* \simeq \left(-i\frac{\gamma_i^*}{2\gamma}A_{s0} + \frac{1}{2}A_{i0}^* \right) \exp[(\gamma-\alpha_s/4)z],$$

$$A_s \simeq \left(i\frac{\gamma_s}{2\gamma}A_{i0}^* + \frac{1}{2}A_{s0} \right) \exp[(\gamma-\alpha_s/4)z] = i(\gamma_s/\gamma_i^*)^{1/2}A_i^* . \tag{32}$$

For practical purposes it is sufficient to have $\gamma\simeq\alpha_s/4$ or $g\simeq\sqrt{2}$. In this case HOPA's can be used as generators and as amplifiers of the signal waves.

We assumed above that the idler field is generated by the process $q\omega_p=\omega_s+\omega_i$. This is equivalent to the assumption that the wave-vector mismatch for all other channels is much larger. In general, the situation is more complicated. There are many different channels that can lead to the generation (or absorption) of the low-frequency idler field. Usually the strongest is the lowest-order generation process, $2\omega_p=\omega_a+\omega_i$ shown in Fig. 19(a). For this particular process one can always produce better phase matching than for the competing lowest-order absorption process $2\omega_p+\omega_i=\omega_c$. Due to a higher-order nonlinearity, the influence of all other processes $q\omega_p=\omega_s\pm\omega_i$ ($q\geqslant4$) on the idler field can be neglected. Assuming that the absorption coefficients α_i, α_a for the idler and additional fields are equal to zero, we can write for the idler amplitude analogous to Eqs. (26)

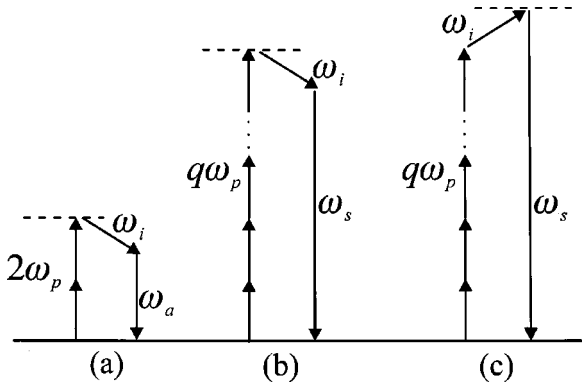

FIG. 19. Schematic illustration of the possibility of gain transfer.

$$A_i^* = B_i^*\exp(i\Delta k_2 z/2),$$

$$B_i^* = -i\frac{\gamma_i^*}{G}A_{a0}\sinh(Gz) + A_{i0}^*\left[\cosh(Gz) - \frac{i\Delta k_2}{2G}\sinh(Gz)\right], \tag{33}$$

where A_{a0}, A_{i0} are the boundary values of the corresponding field amplitudes at $z=0$, $G=\sqrt{\gamma_2^2-(\Delta k_2/2)^2}$,

$$\gamma_i = \frac{2\pi\omega_i}{cn_i}NX_2, \quad \gamma_2 = \frac{2\pi}{c}\left[\frac{\omega_i\omega_a}{n_in_a}\right]^{1/2}N|X_2|, \tag{34}$$

$X_2=d^{NL}(\omega_i)/A_a^*=d_0^{NL}(\omega_i)/A_{a0}^*$, and $\Delta k_2=k_i+k_a-2k_p$. The idler amplitude grows exponentially with the medium length when $|\gamma_2|>|\Delta k_2|/2$ is fulfilled.

For the process shown in Fig. 19(b), the signal amplitude is described by

$$\frac{dA_s}{dz}+\frac{\alpha_s}{2}A_s = i\gamma_sA_i^*\exp[-i\Delta kz],$$

$$\gamma_s = \frac{2\pi\omega_s}{cn_s}N[d_0^{NL}(\omega_s)/A_{i0}^*], \tag{35}$$

where $\Delta k=k_s+k_i-qk_p$. Introducing $a=\alpha_s/2-i\Delta k+i\Delta k_2/2$ and assuming $a^2\neq G^2$, we obtain

$$A_s = \frac{i\gamma_s}{a^2-G^2}\left(aB_i^* - \frac{dB_i^*}{dz}\right)\exp[-i(\Delta k-\Delta k_2/2)z] + C\exp(-\alpha_s z/2),$$

$$C=A_{s0}-\frac{i\gamma_s}{a^2-G^2}[(a+i\Delta k_2/2)A_{i0}^*+i\gamma_i^*A_{a0}], \quad (36)$$

where B_i^* is given by Eq. (33). As can be seen from this expression, at sufficiently large distances ($z\gg 1/G$) the signal amplitude grows exponentially as $A_s\sim\exp(Gz)$ with the gain coefficient determined by the low-order process.

The same is true for the process shown in Fig. 19(c), which is described by

$$\frac{dA_s}{dz}+\frac{\alpha_s}{2}A_s=i\gamma_sA_i\exp[-i\Delta kz],$$

$$\gamma_s=\frac{2\pi\omega_s}{cn_s}N[d_0^{NL}(\omega_s)/A_{i0}], \quad (37)$$

where $\Delta k=k_s-k_i-qk_p$ and A_i is obtained by complex conjugating of Eq. (33). The solution of the above equation is given by

$$A_s=\frac{i\gamma_s}{a^2-G^2}\left(aB_i-\frac{dB_i}{dz}\right)\exp[-i(\Delta k+\Delta k_2/2)z]+C\exp(-\alpha_sz/2),$$

$$C=A_{s0}-\frac{i\gamma_s}{a^2-G^2}[(a-i\Delta k_2/2)A_{i0}-i\gamma_iA_{a0}^*], \quad (38)$$

where now $a=\alpha_s/2-i\Delta k-i\Delta k_2/2$.

It is very important that for the processes shown in Fig. 19, the growth of the high-order signal waves is not limited by their absorption. In this regime, which we call gain transfer, HOPA's can be used as generators. One can also think about the development of synchronously pumped high-order parametric oscillators (HOPO's) with a resonator cavity for idler radiation. We hope that such devices will soon be able to provide higher conversion efficiency in the XUV spectral range than at present.

Concluding this section we note that in an ordinary high-order harmonic generation experiment (with a single pump field) low-order harmonics can automatically serve as idler radiation. In this case parametric amplification of harmonics in the process $2k\omega_p=\omega_{2n+1}+\omega_{2m+1}$ can occur, where $\omega_{2j+1}=(2j+1)\omega_p$, $j=n,m\geqslant 1$, and $k=n+m+1$. Detailed theoretical discussion of this possibility will be published elsewhere [24].

IX. CONCLUSION

Theoretical and experimental investigations of high-order harmonic generation and frequency mixing processes in absorbing, dispersive, and ionizing media have been reported. All factors limiting the frequency conversion efficiency have been analyzed. It has been shown that attenuation of the pump wave can have a dramatic effect on the frequency conversions efficiency. Taking this into account, a very good agreement between the theoretical and experimental results has been obtained. It has been demonstrated that, due to a rapid temporal variation of the wave-vector mismatch during the laser pulse, generation of attosecond pulses is possible.

The development of high-order parametric generators and amplifiers (HOPA's) as a new possibility to improve the frequency conversion efficiency in the XUV spectral range has been considered. High-order parametric amplification has been analyzed taking into account absorption effects. First calculations of the parametric gain coefficients, showing that $\alpha_p\geqslant 1\ \mathrm{cm}^{-1}$ can be obtained, have been performed. Whereas the generation of high-order harmonics is limited by their absorption, HOPA's are free of this limitation due to exponential growth of the idler and signal fields with the medium length.

Further theoretical and experimental efforts are required to realize possibilities considered in this paper.

ACKNOWLEDGMENTS

This work was supported by the Deutsche Forschungsgemeinschaft. We also acknowledge financial support from SFB 407.

[1] A. L'Huillier, X.F. Li, and I.A. Lompre, J. Opt. Soc. Am. B **7**, 527 (1990).
[2] P.L. Shkolnikov, A.E. Kaplan, and A. Lago, Opt. Lett. **18**, 1700 (1993); P.L. Shkolnikov, A. Lago, and A.E. Kaplan, Phys. Rev. A **50**, R4461 (1994); P.L. Shkolnikov, A.E. Kaplan, and A. Lago, J. Opt. Soc. Am. B **13**, 412 (1996).
[3] H.M. Milchberg, C.G. Durfee, III, and T.J. McIlrath, Phys. Rev. Lett. **75**, 2494 (1995).
[4] S. Meyer, H. Eichmann, T. Menzel, S. Nolte, B. Wellegehausen, B.N. Chichkov, and C. Momma, Phys. Rev. Lett. **76**, 3336 (1996).
[5] P. Balcou, P. Salieres, A. L'Huillier, and M. Lewenstein, Phys. Rev. A **55**, 3204 (1997).
[6] H. Lange, A. Chiron, J.-F. Ripoche, A. Mysyrowicz, P. Breger, and P. Agostini, Phys. Rev. Lett. **81**, 1611 (1998).
[7] Z. Chang, A. Rundquist, H. Wang, I. Christov, H.C. Kapteyn, and M.M. Murnane, Phys. Rev. A **58**, R30 (1998).
[8] A. Rundquist, Ch.G. Durfee, III, Z. Chang, C. Herne, S. Backus, M.M. Murnane, and H.C. Kapteyn, Science **280**, 1412 (1998).
[9] E. Constant, D. Garzella, P. Breger, E. Mevel, Ch. Dorror, C. Le Blanc, F. Salin, and P. Agostini, Phys. Rev. Lett. **82**, 1668 (1999).
[10] Y. Tamaki, J. Itatani, Y. Nagata, M. Obara, and K. Midorikawa, Phys. Rev. Lett. **82**, 1422 (1999).
[11] Y. Tamaki, J. Itatani, Y. Nagata, M. Obara, and K. Midorikawa, Phys. Rev. A **59**, 4041 (1999).
[12] M. Schnürer, Z. Cheng, M. Hentschel, G. Tempea, P. Kálmán, T. Brabec, and F. Krausz, Phys. Rev. Lett. **83**, 722 (1999).
[13] Ch.G. Durfee, III, A.R. Rundquist, S. Backus, C. Herne, M.M. Murnane, and H.C. Kapteyn, Phys. Rev. Lett. **83**, 2187 (1999).
[14] K.C. Kulander and T.R. Rescigno, Comput. Phys. Commun.

63, 523 (1991); M. Lewenstein, Ph. Balcou, M.Y. Ivanov, A. L'Huillier, and P.B. Corkum, Phys. Rev. A **49**, 2117 (1994).

[15] G.V. Marr and J.B. West, At. Data Nucl. Data Tables **18**, 497 (1976); J.J. Yeh and I. Lindau, *ibid.* **32**, 1 (1985); B.L. Henke, E.M. Gullikson, and J.C. Davis, *ibid.* **54**, 181 (1993); J.A.R. Samson, Z.X. He, L. Yin, and G.N. Haddad, J. Phys. B **27**, 887 (1994); www.pa.uky.edu/~verner/photo.html; www-cxro.lbl.gov/optical constants/pert form.html

[16] A.M. Perelomov, V.S. Popov, and M.V. Terent'ev, Zh. Éksp. Teor. Fiz. **50**, 1393 (1966) [Sov. Phys. JETP **23**, 924 (1966)].

[17] N.B. Delone and V.P. Krainov, J. Opt. Soc. Am. B **8**, 1207 (1991).

[18] H.J. Lehmeier, W. Leupacher, and A. Penzkofer, Opt. Commun. **56**, 67 (1985); M. Nisoli, S. De Silvestri, and O. Svelto, Appl. Phys. Lett. **68**, 2793 (1996); E.T.J. Nibbering, G. Grillon, M.A. Franco, B.S. Prade, and A. Mysyrowicz, J. Opt. Soc. Am. B **14**, 650 (1997).

[19] E.A.J. Marcatili and R.A. Schmeltzer, Bell Syst. Tech. J. **43**, 1783 (1964).

[20] S. A. Akhmanov, V. A. Vysloukh, and A. S. Chirkin, *Optics of Femtosecond Laser Pulses* (AIP, New York, 1992).

[21] V.P. Krainov, J. Opt. Soc. Am. B **14**, 425 (1997); A. Scrinzi, M. Geissler, and T. Brabec, Phys. Rev. Lett. **83**, 706 (1999).

[22] S. Meyer, B.N. Chichkov, and B. Wellegehausen, J. Opt. Soc. Am. B **16**, 1587 (1999).

[23] Y.R. Shen, *The Principles of Nonlinear Optics* (Wiley, New York, 1984); R.W. Boyd, *Nonlinear Optics* (Academic Press, San Diego, CA, 1992).

[24] B.N. Chichkov, S. Meyer, and B. Wellegehausen (unpublished).